Hindawi
Advances in Meteorology
Volume 2017, Article ID 8434020, 10 pages
https://doi.org/10.1155/2017/8434020

Research Article

Ecosystem Drought Response Timescales from Thermal Emission versus Shortwave Remote Sensing

Erika Andujar,[1] Nir Y. Krakauer,[1,2] Chuixiang Yi,[2,3] and Felix Kogan[4]

[1]*Department of Civil Engineering, The City College of New York, City University of New York, New York, NY, USA*
[2]*Program in Earth and Environmental Sciences, The Graduate Center, City University of New York, New York, NY, USA*
[3]*Department of Earth and Environmental Sciences, Queens College, City University of New York, Flushing, New York, NY, USA*
[4]*NOAA/NESDIS, College Park, MD, USA*

Correspondence should be addressed to Nir Y. Krakauer; nirkrakauer@gmail.com

Received 12 May 2017; Revised 2 September 2017; Accepted 26 September 2017; Published 25 October 2017

Academic Editor: Panuganti C. S. Devara

Remote sensing is used for monitoring the impacts of meteorological drought on ecosystems, but few large-scale comparisons of the response timescale to drought of different vegetation remote sensing products are available. We correlated vegetation health products derived from polar-orbiting radiometer observations with a meteorological drought indicator available at different aggregation timescales, the Standardized Precipitation Evapotranspiration Index (SPEI), to evaluate responses averaged globally and over latitude and biome. The remote sensing products are Vegetation Condition Index (VCI), which uses normalized difference vegetation index (NDVI) to identify plant stress, Temperature Condition Index (TCI), based on thermal emission as a measure of surface temperature, and Vegetation Health Index (VHI), the average of VCI and TCI. Globally, TCI correlated best with 2-month timescale SPEI, VCI correlated best with longer timescale droughts (peak mean correlation at 13 months), and VHI correlated best at an intermediate timescale of 4 months. Our results suggest that thermal emission (TCI) may better detect incipient drought than vegetation color (VCI). VHI had the highest correlations with SPEI at aggregation times greater than 3 months and hence may be the most suitable product for monitoring the effects of long droughts.

1. Introduction

Drought reduces access to water supplies, leading to malnutrition and famine as well as disturbances in ecosystems [1–3]. As a result of anthropogenic global warming, it is expected that the frequency and intensity of drought will increase in many areas of the world [1], driven by reductions in precipitation and increased evapotranspiration from higher temperatures [2]. An analysis of historic observations has found increases in drought-affected land area [3], consistent with climate model projections of increases in aridity and droughts [4].

A major concern associated with drought effects is change in ecosystem dynamics as a result of mortality of trees and other plants [5–8], which can lead to alterations in plant community composition, species distributions, and carbon [9–11] and water cycling [12]. The goal of this study is to determine how long meteorological drought takes to manifest globally and in croplands, grasslands, and evergreen broadleaf forest ecosystems, based on remotely sensed Vegetation Health Product (VHP) data. An advantage of drought monitoring with remote sensing data compared to ground observations is the ease with which global studies can be performed, since the availability of data is not dependent on monitoring station distribution or international cooperation.

In general, remote sensing can be applied to drought monitoring by choosing surface radiative properties related to vegetation stress or soil moisture status [13]. The VHPs include Temperature Condition Index (TCI) and Vegetation Condition Index (VCI). VCI uses a ratio of land surface reflectivity in visible and near infrared wavelengths, the normalized difference vegetation index (NDVI), to assess coverage of healthy vegetation, while TCI uses thermal infrared emission to assess land surface temperature (LST). These VHPs, obtained from NOAA's Advanced Very High Resolution Radiometer (AVHRR) sensor data, are available

from the NOAA STAR Global Vegetation Health Products website [14], with data since the early 1980s. Validation with ground measurements in several parts of the world has shown these indices to be successful for assessing drought impact [4].

The ecosystems chosen for special examination of the effects of meteorological drought on remotely sensed VHPs in this study include cropland, grassland, and evergreen broadleaf forests. Croplands are important because people utilize these 1.47–1.53 billion hectares of land [15] for food consumption, livestock feed, bioenergy, chemical feedstocks, and biopharmaceuticals [16]. Stagnation of the world's grain production and increases in drought occurrence with global warming may make it harder for demands to be met [12].

Grassland ecosystems support grazing livestock, sequester carbon, catch water, and preserve ecosystem biodiversity, as well as creating livelihood for many low-income people [9]. Grasslands can act as carbon sources or sinks depending on water availability, in that they release carbon in dry years but store carbon during normal or wet years [17, 18].

Forest biomes contain about 80% of Earth's total plant biomass [19] and in 2010 it was estimated that the total carbon stock in the world's forests was 289 Gt C [20]. When extreme climate conditions prevail, evergreen broadleaf forests, which include tropical rainforests, build less soil organic carbon [21] and sequester less atmospheric carbon [10]. Estimates suggest an average reduction of forest canopy photosynthetic capacity due to unfavorable climate extremes of 6.3 Gt C per year over 2001–2010, with evergreen broadleaf forests contributing to 52% of the total reduction [10].

Most previous studies of drought response timescales have been local (e.g., north-eastern Spain, parts of the United States, Thailand) or limited to select ecosystems or plant species (e.g., conifer forests in the southwest United States) [22–28]. A number of these studies indicate that there is variation in the strength and lag time of peak correlation between precipitation and remotely sensed LST and land surface reflectivity indices for different ecosystems. In the Great Plains of the United States, the strongest correlation between LST and Departure from Normal Precipitation index was found at a 2-3-month timescale, as compared to a timescale greater than 6 months for NDVI [23]. This was observed for grassland, cropland, and the Great Plains area as a whole [23]. In southern Africa, NDVI of trees was less sensitive than NDVI of grass to interannual variations in precipitation, a difference attributed to trees' deep roots affording them more steady access to soil moisture [29].

Additionally, humid and arid biomes have been found to have shorter response times than semiarid and subhumid biomes [30]. Some studies have shown a stronger correlation between reflectivity remote sensing products and precipitation indices than between thermal products and precipitation indices [24, 25].

In terms of correlations with meteorology, TCI demonstrates stronger correlation with above ground temperature [4], while VCI is better correlated to cumulative seasonal rainfall [26] and responds most to prolonged moisture stress [27] as it affects photosynthetic activity and plant health. As a result of the nature of the two indices, and the findings of previous studies, it is hypothesized that the response timescale to meteorological drought onset will be shorter for TCI than for VCI and that the response of remote sensing based indicators to drought will vary depending on ecosystem.

A number of meteorological drought indicators have been employed. The indicator used here is the Standardized Precipitation Evapotranspiration Index (SPEI), which is based on anomalies in monthly average precipitation (P) minus reference evapotranspiration (or atmospheric evaporative demand; ET_0) [31–33]. ET_0 can be calculated using one of several available formulas, based on temperature and possibly also wind speed, sunniness, and other climatic variables. The aggregation of P minus ET_0 for a set of n months, followed by standardization to a multiyear zero mean and unit standard deviation, yields SPEI for different timescales [32]. SPEI is available globally at aggregation timescales n ranging from 1 to 48 months in SPEIbase [34], making it possible to assess both long- and short-term drought [28]. The effects of evapotranspiration in the water balance are important because temperature influences water availability in the environment [35] and should also be considered as contributing to meteorological drought [3, 36, 37]. The inclusion of evaporative demand in SPEI is an improvement for drought assessment over earlier indicators such as Standardized Precipitation Index [38] that do not explicitly account for temperature, and SPEI is therefore used in a number of recent studies of drought risk assessment and seasonal prediction [28, 39, 40].

2. Methods

The datasets used in this investigation are summarized in Table 1.

As mentioned above, TCI and VCI are two VHPs derived from remote sensing that are commonly used for drought monitoring. The TCI and VCI datasets used are based on data from AVHRR as processed by the NOAA STAR Global Vegetation Health Products group [14]. TCI is based on thermal emissions measured at infrared wavelengths and is calculated as

$$\mathrm{TCI}_j = \frac{\mathrm{BT}_{\max} - \mathrm{BT}}{\mathrm{BT}_{\max} - \mathrm{BT}_{\min}} \times 100, \quad (1)$$

where TCI_j is the TCI value for week j, BT is the smoothed brightness temperature for week j, and $\mathrm{BT}_{\max}$ and $\mathrm{BT}_{\min}$ are the multiyear maximum and minimum brightness temperature observed for that week (based on a 25-year climatology that includes our study period) [4, 41, 42].

VCI is calculated using NDVI, which is based on the difference in reflectivity of green vegetation cover between red and near infrared wavelengths, according to the formula

$$\mathrm{VCI}_j = \frac{\mathrm{NDVI} - \mathrm{NDVI}_{\min}}{\mathrm{NDVI}_{\max} - \mathrm{NDVI}_{\min}} \times 100, \quad (2)$$

where VCI_j is the VCI value for week j. NDVI is the smoothed weekly NDVI, and $\mathrm{NDVI}_{\min}$ and $\mathrm{NDVI}_{\max}$ are the multiyear minimum and maximum observed NDVI at the

Table 1: Summary of the spatial and temporal characteristics of the products used.

Product	Years available	Space resolution	Time resolution
SPEI (1–48 months' timescale)	1901–2014	0.5°	Monthly
VCI, TCI, VHI	1982–2016	0.144°	Weekly
MODIS (MCD12Q1)	2000-2001	0.5°	One time

same week. VCI and TCI range from 0 to 100. Values below 40 indicate stressed vegetation conditions, often due to drought [26]. See [4] for details of the preprocessing and smoothing of the AVHRR NDVI and BT series used to construct TCI and VCI.

A third VHP evaluated was Vegetation Health Index (VHI). This is defined as the average of TCI and VCI and hence combines information from surface reflectance and brightness temperature [41]. Weekly VHP data (for TCI, VCI, and VHI) were obtained from the 0.144° (~16 km resolution) NOAA STAR Vegetation Health dataset.

Monthly SPEI data were acquired from the Global SPEI Database, SPEIbase, for 1982–2014 and aggregation timescales of 1–48 months at a spatial resolution of 0.5° [34]. The SPEI was calculated using University of East Anglia Climate Research Unit (CRU) gridded monthly precipitation and reference evapotranspiration data [43], with the P minus ET_0 values transformed to standard normal distributions using the log-logistic distribution fitted with the unbiased probability weighted moments method [33]. ET_0 is calculated by CRU using the Food and Agricultural Organization (FAO) Penman-Monteith method for potential evapotranspiration from a well-watered grass surface [34].

To delineate ecosystem types, the Moderate Resolution Imaging Spectroradiometer (MODIS) International Satellite Land Surface Climatology (ISLSCP) Initiative II data collection land cover product [44, 45] with a 0.5° resolution was used. This is based on the 1 km MODIS land use product (MOD12Q1), which used remote sensing data collected from October 2000 to October 2001 and a decision tree machine-learning method for classification of each pixel into one of 18 land cover categories, including evergreen broadleaf forest, grassland, and cropland. It was upscaled to 0.5° by choosing the most common land cover within each 0.5° cell as the descriptor for that cell.

The years for which VHP and SPEI data were both available are 1982–2014. The VHP dataset has some gaps (1984, 1985, 1988, 1994, and 2004) due to unavailable remote sensing data. These missing values were simply not included in the correlation analysis. The SPEI dataset did not have missing values.

Because the monthly SPEI product reflects precipitation and reference evaporation integrated over the whole month (and, depending on aggregation time, also previous months), it strictly speaking is a measure of moisture status as of the end of the month. Therefore, for the most consistent comparison with SPEI, we used only the VHP values from the weeks that include the end of each month, representing each VHP index's value at the end of the month.

Given the finer spatial resolution of the VHP datasets, compared to the SPEI dataset, they were upscaled to a final spatial resolution of 0.5° by area-weighted averaging of all VHP pixels falling within an SPEI pixel. Pearson correlations were then obtained for each pixel and calendar month between TCI, VCI, or VHI and SPEI at different aggregation timescales, and the correlations then averaged across calendar months for each pixel and then across all pixels in a biome (or globally). We also show maps of the correlation of SPEI with TCI and VCI and figures of mean correlation by latitude for the aggregation timescale when the global mean correlation is maximal. Note that the global means are averaged across all pixels with valid VHP values, regardless of biome. We exclude from our analyses VHP pixels flagged as (1) desert areas with little vegetation, (2) snow and ice covered areas, or (3) cold-season months in mountain and high-latitude areas that are outside the growing season.

To check the sensitivity of our results to the averaging process, a different Pearson correlation analysis was also performed where values for each pixel were computed by finding the correlation between SPEI and VHP across all calendar months, rather than the correlation being computed for each month separately. Similar results were found (not shown).

Averaging correlations mean that negative correlations offset positive ones in determining the mean. If plants grow better when more moisture is available, we would expect generally positive correlations between the VHPs and SPEI, with any negative correlations obtained being only due to sampling error. However, as will be discussed below, negative correlations between VHPs and SPEI are also biophysically plausible under some conditions. To assess the effect of averaging across correlations of opposite sign, we conducted a supplementary analysis where correlations were averaged only after either setting all negative values to zero or setting all positive values to zero. We refer to these as positive-only and negative-only mean correlations.

To quantify the significance of the mean correlation coefficients found, we conducted a Monte Carlo analysis where these were computed (i.e., means by pixel, biome, latitude band, and globally) for 100 random permutations of the months of the SPEI time series. After random permutation of the SPEI, the expected value of all correlations with VHPs is zero. Therefore, we used the 95th percentile of the absolute value of the mean correlations under permutation as the threshold for determining that the actually observed correlations were significantly different from zero (i.e., unlikely if there was no underlying relationship between SPEI and the VHPs).

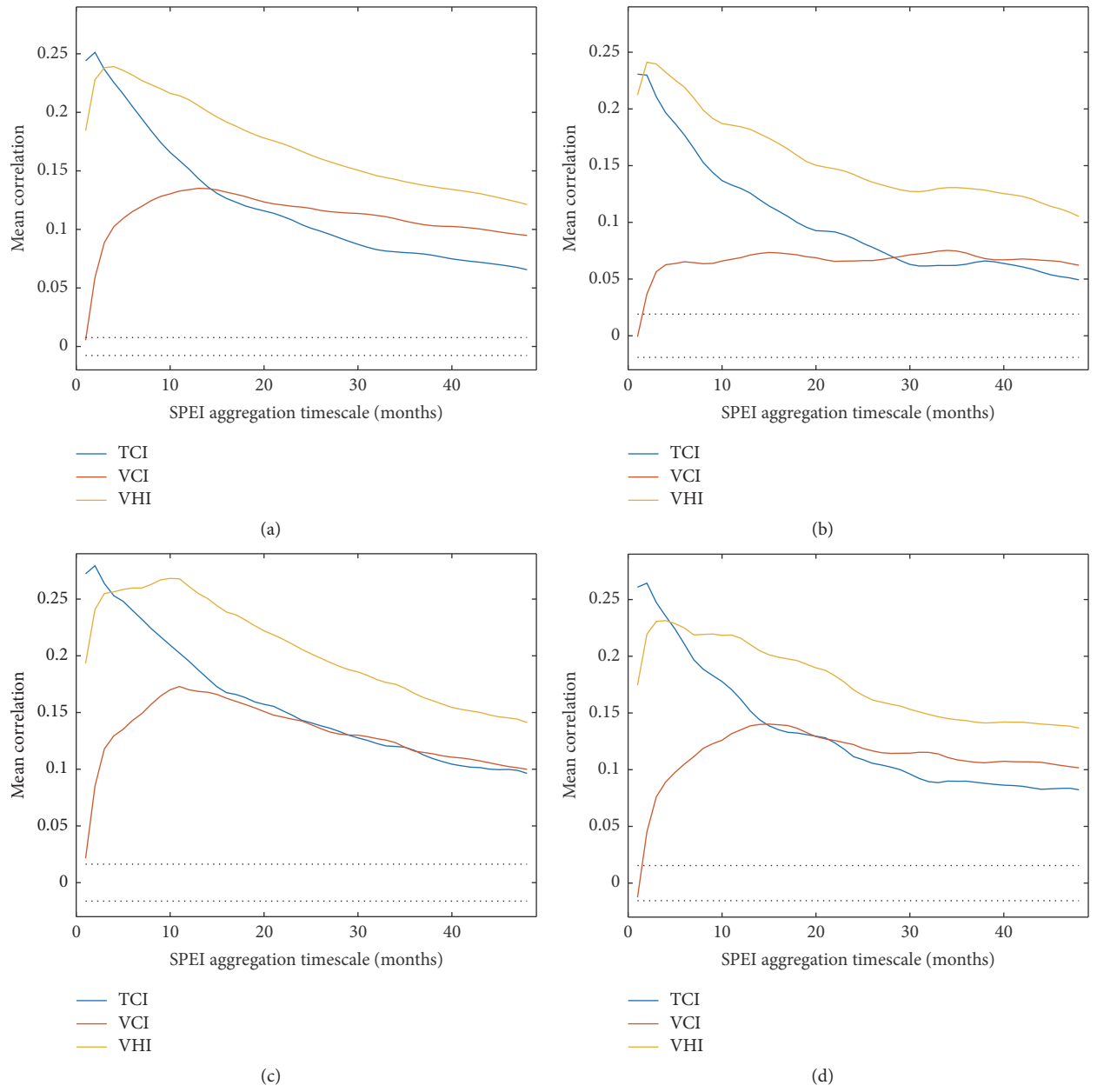

FIGURE 1: TCI, VCI, and VHI mean correlation globally with SPEI at different aggregation timescales. (a) Global mean, (b) evergreen broadleaf forest, (c) grassland, and (d) cropland. The dotted lines show the range over which mean correlations would be not significantly different from zero, as estimated from Monte Carlo simulations of sample correlation sizes.

3. Results

The mean global correlations of the VHPs with SPEI at different timescales are shown in Figure 1(a). Correlation with TCI peaked at 0.25, for an SPEI aggregation timescale of 2 months, and decreased gradually as aggregation timescale increased. Correlation with VCI increased more gradually and was smaller, peaking at 0.14 at an SPEI aggregation timescale of 13 months. Correlation with VHI peaked at 0.24 for a timescale of 4 months and for that timescale and longer ones was consistently higher than the correlation of SPEI at the same timescales with TCI or VCI, indicating that the combination of TCI and VCI may be more consistently sensitive to longer timescale moisture conditions than either index alone.

For evergreen broadleaf forest, mean correlation with TCI peaked at 0.23 at the 1-month SPEI timescale, while correlation with VCI was consistently rather low, peaking at 0.08 at 34 months, and VHI peaked at 0.24 at 3 months (Figure 1(b)). For grassland, mean correlation with TCI peaked at 0.28 at the 2-month SPEI timescale, while VCI peaked at 0.17 at 11 months, and VHI peaked at 0.27 at 10 months (Figure 1(c)). For cropland, mean correlation with TCI peaked at 0.26 at the 2-month SPEI timescale, while

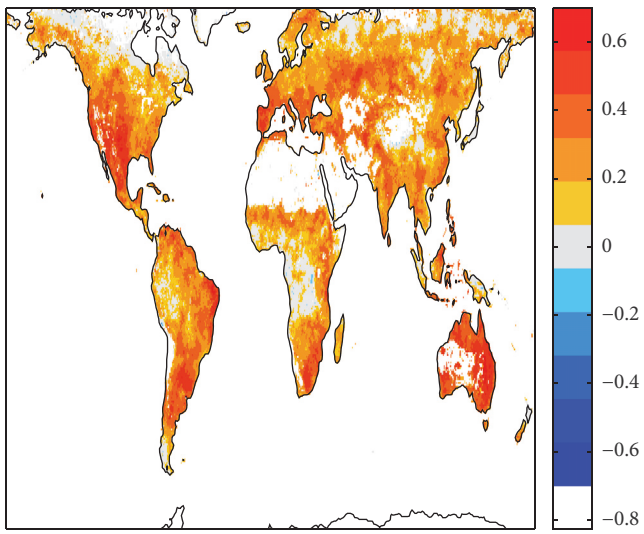

Figure 2: Map of TCI correlation with 2-month aggregation timescale SPEI (when the peak TCI correlation occurred for the global mean). Pixels with nonsignificant correlations are left gray.

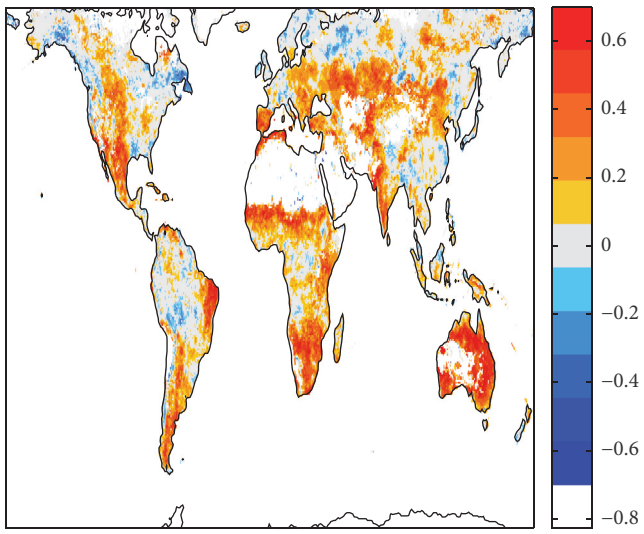

Figure 3: Map of VCI correlation with 13-month aggregation timescale SPEI (when the peak VCI correlation occurred for the global mean). Pixels with nonsignificant correlations are left gray.

VCI peaked at 0.14 at 15 months, and VHI peaked at 0.23 at 4 months (Figure 1(d)). While the mean correlations for individual biomes thus showed some differences from the global mean, TCI was consistently most strongly correlated with short-term moisture status (1- or 2-month SPEI), while VCI correlation was greatest with SPEI aggregation time of 11 months or above. VHI correlation peaked at an SPEI timescale of 3–10 months, intermediate between those of TCI and VCI, and was higher than either the TCI or VCI correlation at the longer SPEI aggregation times.

Mapping the TCI correlation with 2-month aggregation timescale SPEI (Figure 2) indicates that most of the land surface has a positive correlation, while areas at higher latitude and some equatorial rainforests have near zero correlation coefficients. It can be seen that western North America, eastern South America, the eastern edge of Africa, and large portions of Europe, Russia, and Australia have high positive correlation coefficients of TCI with the moisture index SPEI, in the range of 0.4–0.7.

Some of the highest correlations between VCI and 13-month aggregation timescale SPEI are found in semiarid portions of South America, North America, Africa, and Central and Southwest Asia (Figure 3). VCI correlation with SPEI is also high in Australia. However, north of 50°N and even in some moister areas at lower latitudes (such as the southeast USA, portions of south China, Bangladesh, and many equatorial rainforests), the correlation between SPEI and VCI is more commonly near zero or negative.

It is also possible to map the VHP correlations with SPEI at any other available aggregation timescale. For example, VCI is generally less positively correlated with SPEI at the 2-month aggregation timescale, compared with the 13-month timescale (Figure 4). Large positive correlations are still found in semiarid grasslands of South America, Africa, Australia, North America, and Central Asia, but compared to the 13-month timescale, significant negative correlations are more

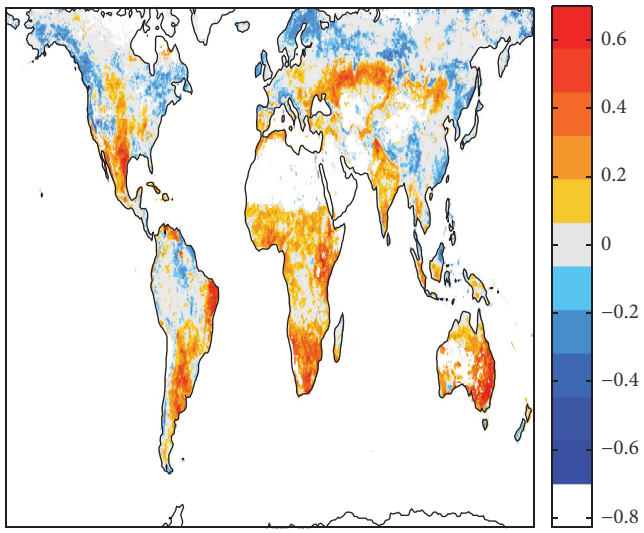

Figure 4: Map of VCI correlation with 2-month aggregation timescale SPEI (when the peak TCI correlation occurred for the global mean). Pixels with nonsignificant correlations are left gray.

widespread in temperate and boreal forest regions of Eurasia and North America.

The TCI correlation with 2-month aggregation timescale SPEI as averaged by latitude (Figure 5) increases from 50°S to 30°S and then decreases from 30°S to 10°S latitude, where the peak average correlation is above 0.4 around 30°S. The correlation then increases going northward from the Equator and reaches above 0.3 before decreasing poleward of 40°N. This can be understood as vegetation in subtropical, arid, or semiarid zones (which include much of the grassland and cropland biomes) being more sensitive to meteorological drought than vegetation in moist equatorial and cool high-latitude ecosystems.

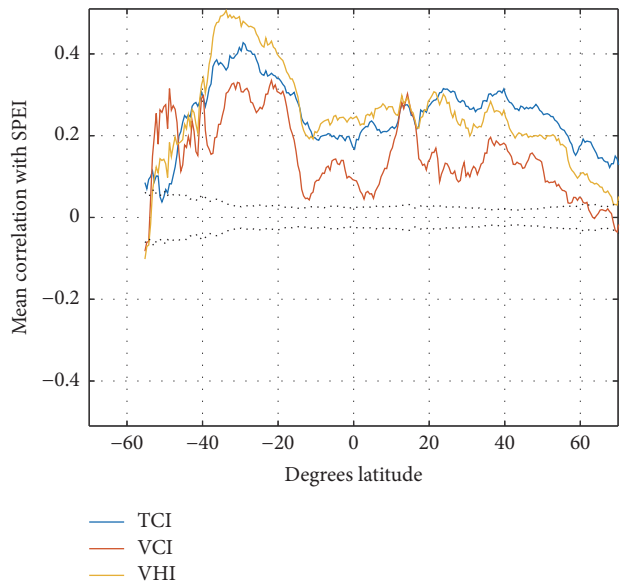

Figure 5: Average correlation for TCI (with SPEI at 2-month aggregation timescale), VCI (with 13-month timescale SPEI), and VHI (with 4-month timescale SPEI) by latitude. The aggregation times shown are those for which the global mean correlations are highest. The dotted lines show the range over which mean correlations would be not significantly different from zero. This range broadens at high southern latitudes because fewer pixels are available there for averaging.

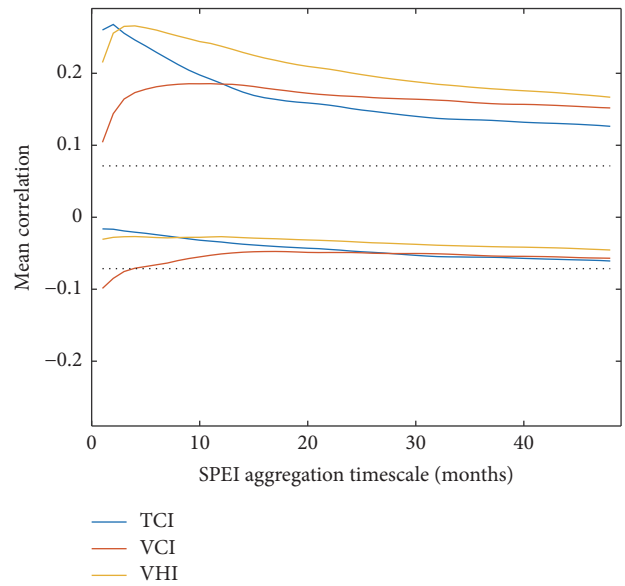

Figure 6: TCI, VCI, and VHI positive-only and negative-only mean correlations globally with SPEI at different aggregation timescales. For the positive-only average, all negative correlations were set to zero, while, for the negative-only average, all positive correlations were set to zero. The dotted lines show the range over which the means would be not significantly different from zero.

Similar to TCI, VCI shows different average correlations with SPEI according to latitude (Figure 5). In the latitudes between 50°S and 20°S, the correlation increases from −0.1 to a peak of ~0.3. Continuing north, the correlation decreases to under 0.1 near the Equator (consistent with the low mean correlations with SPEI for VCI in evergreen broadleaf forests) and then increases again to above 0.2 between 10 and 20°N and a smaller peak between 30 and 40°N, before steadily decreasing to reach zero near the Arctic Circle.

VHI shows more steady mean correlations with 4-month timescale SPEI, staying in the range 0.2–0.3 between ~15°S and ~50°N, peaking at almost 0.5 around 30°S, and decreasing toward zero going poleward (Figure 5).

The positive-only and negative-only global mean correlations are shown in Figure 6. The positive-only mean was, as would be expected, somewhat larger than the overall mean shown in Figure 1. The pattern of correlation as a function of SPEI aggregation time was similar to that of the overall mean, with VHI and VCI peaking at successively longer aggregation times compared to TCI. The peak positive-only mean correlations were found at 2 months for TCI, 4 months for VHI, and 11 months for VCI. The negative-only means were smaller in magnitude and were most pronounced for VCI and at short SPEI aggregation times. For VHI and TCI, the magnitude of the negative-only means was within the range inferred from Monte Carlo simulations where all underlying correlations were zero, implying that their negative correlations with SPEI are not widespread or large enough to be easily discerned in our data.

4. Discussion

The findings of this study suggest that TCI globally responds most to shorter-timescale drought (with mean correlation with SPEI peaking at an aggregation timescale of 1 or 2 months for all biomes in this study) and had higher peak correlations than VCI did, while VCI responded most to long droughts (with higher correlations at longer aggregation timescales for SPEI). Differences between the shorter response time of TCI and longer response time of VCI can possibly be attributed to the biophysical changes that vegetation must undergo for the effect of drought to be detected by VCI, in contrast to changes in land surface temperature detected by TCI that are largely due to physical and physiological suppression of evaporation and transpiration when less water is available and are thus more immediate. TCI's stronger correlation with SPEI can also be partly attributed to the common temperature component the two indices share, since higher temperature increases reference evaporation in the SPEI calculation as well as increasing the remotely sensed thermal emission.

Differences in the strength of the correlation between VCI and TCI with SPEI between different biomes may ultimately be the result of their different latitude and climate zone distributions, which are associated with different plant functional types and adaptations needed to endure drought. For example, plants of arid regions have mechanisms that make it possible for them to rapidly adapt to changing water availability, while plants in humid biomes usually have poor adaptability to water shortage, and plants of semiarid and subhumid biomes may respond only to longer droughts

because they are adapted to withstand frequent water deficits [30]. SPEI has previously been shown to have low correlation with NDVI in low latitudes [30], potentially a result of the generally positive water balance in the deep tropics, which means that drought serious enough to affect vegetation condition is not common. SPEI also has low correlation with NDVI in the higher latitudes, where the primary limiting factor for vegetation activity is sunlight and water limitation tends to be less critical. The evergreen broadleaf forest ecosystem was found here to have the lowest correlation with SPEI for both VCI and TCI, consistent with it being mostly located in the tropics, where mean precipitation is quite high and therefore drought does not frequently reduce NDVI. Additionally, the evergreen broadleaf forest ecosystems may be more resistant to drought because the deep roots that the trees in these forests have allow them to reach subsurface water reservoirs to offset drought effects [46–48]. Deep soils and roots can buffer plant response to lower water availability [49, 50]. Shallow groundwater and fractured rocks offer additional water stores that plant roots can tap [51, 52]. We may hypothesize that in places where soil conditions and plant type allow drawing on a large water reservoir, NDVI would be disproportionately affected by long meteorological droughts (reflected by SPEI at long aggregation periods) and not by short droughts. Determining the sensitivity of VHPs to drought of various timescales (as quantified by low SPEI) could be used to map rooting depth of different vegetation types [53, 54].

In places, we found negative correlations of VHPs with SPEI, which means that in those places vegetation health tends to be better under drier than average conditions. These negative correlations were particularly widespread for VCI correlated with short-timescale SPEI (Figure 4). In general, depending on the prevailing climate, plant growth can be limited by either water, cold temperature, or light availability [55]. In water-limited climates, such as those found in many grassland areas, we expect more plant growth when ample moisture is available (high SPEI), resulting in a positive correlation of VHPs with SPEI. In temperature or light limited climates, such as many evergreen broadleaf and boreal forests, having more moisture than usual available would not help plant growth and may even impede it if wetter conditions are associated with cooler temperatures and less incoming sunlight. In such locations, we would expect a negative correlation between VHPs and SPEI. Similarly, the cooling and haze following volcanic eruptions are found to negatively affect tree growth at high latitudes (temperature and light limited conditions) but not at low latitudes (moisture limited conditions) [56], and Amazon rainforest trees grow more during the dry season, when more sunlight is available and there is still adequate moisture compared to during the wet season [57]. For TCI, which measures surface temperature, the decreased correlation of surface air temperature with antecedent precipitation as climate gets cooler and more moist and evaporation becomes limited by energy availability rather than water availability [58, 59] would also make the correlation with SPEI less positive at high latitudes and equatorial rain forests, consistent with what we find.

We note that as a result of global warming, more regions are projected to shift to moisture-limited growing conditions [11, 60], which would imply that correlations of VHPs with SPEI would become more positive over time. This hypothesis could be tested in future work.

Our findings suggest that VHPs globally work best as drought indicators in semiarid areas, most prevalent in the midlatitudes (15–45°N and S). We also observed that VHI, which is the average of VCI and TCI, generally worked better than both VCI and TCI as a drought indicator at longer timescales (SPEI aggregation timescale greater than 3 months).

A source of uncertainty in this study is the resampling of the VHP data to a coarser resolution of 0.5° (~50 km), which could be avoided by using finer resolution meteorological and land cover datasets. Finer resolution would also allow better differentiation between land covers that are intermixed. The VHPs are available from NOAA at 0.04° (~4 km) resolution, a finer spatial scale which would be helpful for studies of individual regions and ecosystems. VHPs becoming available for the last few years offer even finer spatial resolution [61]. Climate data at finer temporal resolution would also enable study of the climate response of VHPs over submonthly timescales, which could be particularly relevant for better understanding the fast TCI response. For cropland, it would also be helpful to distinguish irrigated from rain-fed agriculture [62, 63], as well as other cropping and management practices [64–66] that would affect sensitivity to meteorological drought.

Additionally, there are many other factors aside from drought that can degrade vegetation, such as fires, pests, or disease, which may not correlate with SPEI but still affect the remote sensing vegetation health products. This can help explain the low correlation magnitudes with SPEI seen with TCI and especially VCI at many pixels.

5. Conclusions

This study aimed to determine the typical response of the remotely sensed VCI, TCI, and VHI products to different lengths of meteorological drought globally and for croplands, grasslands, and evergreen broadleaf forest ecosystems. Through analyses of their correlation with the meteorological drought indicator SPEI, differences in the response to drought of different lengths between TCI and VCI were found globally and for the different ecosystems. At the global and ecosystem scales, we observed that TCI had its strongest correlation with SPEI for shorter drought periods, while VCI's sensitivity was greater for longer droughts. This may make TCI better suited for earlier-stage drought monitoring, while VHI, the average of VCI and TCI, may be the most suitable for monitoring the effects of long droughts.

Disclosure

All statements made are not the opinions of the funding agency or the US government but reflect the authors' views.

Conflicts of Interest

The authors declare no conflicts of interest.

Authors' Contributions

All the authors conceived and designed the analyses; Erika Andujar and Nir Y. Krakauer performed the analyses and wrote the paper.

Acknowledgments

This study was supported by National Oceanic and Atmospheric Administration (NOAA) under Grants NA16SEC4810008 and NA15OAR4310080.

References

[1] , *Climate Change 2007—Impacts, Adaptation and Vulnerability: Working Group II Contribution to the Fourth Assessment Report of the IPCC*, M. L. Parry, Ed., Cambridge University Press, Cambridge, UK, 2007.

[2] J. Sheffield and E. F. Wood, "Projected changes in drought occurrence under future global warming from multi-model, multi-scenario, IPCC AR4 simulations," *Climate Dynamics*, vol. 31, no. 1, pp. 79–105, 2008.

[3] A. Dai, "Characteristics and trends in various forms of the Palmer Drought Severity Index (PDSI) during 1900–2008," *Journal of Geophysical Research*, vol. 116, Article ID D12115, 2011.

[4] F. N. Kogan, "Global drought watch from space," *Bulletin of the American Meteorological Society*, vol. 78, no. 4, pp. 621–636, 1997.

[5] D. D. Breshears, N. S. Cobb, P. M. Rich et al., "Regional vegetation die-off in response to global-change-type drought," *Proceedings of the National Acadamy of Sciences of the United States of America*, vol. 102, no. 42, pp. 15144–15148, 2005.

[6] A. M. Schwantes, J. J. Swenson, and R. B. Jackson, "Quantifying drought-induced tree mortality in the open canopy woodlands of central Texas," *Remote Sensing of Environment*, vol. 181, pp. 54–64, 2016.

[7] P. J. Van Mantgem, N. L. Stephenson, J. C. Byrne et al., "Widespread increase of tree mortality rates in the Western United States," *Science*, vol. 323, no. 5913, pp. 521–524, 2009.

[8] A. R. Gitlin, C. M. Sthultz, M. A. Bowker et al., "Mortality gradients within and among dominant plant populations as barometers of ecosystem change during extreme drought," *Conservation Biology*, vol. 20, no. 5, pp. 1477–1486, 2006.

[9] M. Boval and R. M. Dixon, "The importance of grasslands for animal production and other functions: a review on management and methodological progress in the tropics," *Animal*, vol. 6, no. 5, pp. 748–762, 2012.

[10] S. Wei, C. Yi, G. Hendrey et al., "Data-based perfect-deficit approach to understanding climate extremes and forest carbon assimilation capacity," *Environmental Research Letters*, vol. 9, no. 6, Article ID 065002, 2014.

[11] C. Yi, S. Wei, and G. Hendrey, "Warming climate extends dryness-controlled areas of terrestrial carbon sequestration," *Scientific Reports*, vol. 4, article 5472, 2014.

[12] F. A. Ward, "Economic impacts on irrigated agriculture of water conservation programs in drought," *Journal of Hydrology*, vol. 508, pp. 114–127, 2014.

[13] M. Choi, J. M. Jacobs, M. C. Anderson, and D. D. Bosch, "Evaluation of drought indices via remotely sensed data with hydrological variables," *Journal of Hydrology*, vol. 476, pp. 265–273, 2013.

[14] NOAA STAR, Global vegetation health products, 2016.

[15] P. S. Thenkabail, M. A. Hanjra, V. Dheeravath, and M. Gumma, "A holistic view of global croplands and their water use for ensuring global food security in the 21st century through advanced remote sensing and non-remote sensing approaches," *Remote Sensing*, vol. 2, no. 1, pp. 211–261, 2010.

[16] D. R. Ort, S. S. Merchant, J. Alric et al., "Redesigning photosynthesis to sustainably meet global food and bioenergy demand," *Proceedings of the National Acadamy of Sciences of the United States of America*, vol. 112, no. 28, pp. 8529–8536, 2015.

[17] C. Yi, G. Rustic, X. Xu et al., "Climate extremes and grassland potential productivity," *Environmental Research Letters*, vol. 7, no. 3, Article ID 035703, 2012.

[18] L. Zhang, B. K. Wylie, L. Ji, T. G. Gilmanov, L. L. Tieszen, and D. M. Howard, "Upscaling carbon fluxes over the Great Plains grasslands: sinks and sources," *Journal of Geophysical Research: Biogeosciences*, vol. 116, no. 3, Article ID G00J03, 2011.

[19] Y. Pan, R. A. Birdsey, O. L. Phillips, and R. B. Jackson, "The structure, distribution, and biomass of the world's forests," *Annual Review of Ecology, Evolution and Systematics*, vol. 44, pp. 593–622, 2013.

[20] FAO, "Global forest resources assessment 2010," Tech. Rep., Food and Agriculture Organization of the United Nations, Rome, Italy, 2010.

[21] T. Chiti, E. Díaz-Pinés, and A. Rubio, "Soil organic carbon stocks of conifers, broadleaf and evergreen broadleaf forests of Spain," *Biology and Fertility of Soils*, vol. 48, no. 7, pp. 817–826, 2012.

[22] E. Pasho, J. J. Camarero, M. de Luis, and S. M. Vicente-Serrano, "Impacts of drought at different time scales on forest growth across a wide climatic gradient in north-eastern Spain," *Agricultural and Forest Meteorology*, vol. 151, no. 12, pp. 1800–1811, 2011.

[23] Z. Wan, P. Wang, and X. Li, "Using MODIS Land Surface Temperature and Normalized Difference Vegetation Index products for monitoring drought in the southern Great Plains, USA," *International Journal of Remote Sensing*, vol. 25, no. 1, pp. 61–72, 2004.

[24] S. Bunrit, R. Chanklan, S. Boonamnuay, N. Kerdprasop, and K. Kerdprasop, "Neural network-based analysis of precipitation and remotely sensed data," in *Proceedings of the International MultiConference of Engineers and Computer Scientists*, vol. 1, Hong Kong, March 2016.

[25] Y. Bayarjargal, A. Karnieli, M. Bayasgalan, S. Khudulmur, C. Gandush, and C. J. Tucker, "A comparative study of NOAA-AVHRR derived drought indices using change vector analysis," *Remote Sensing of Environment*, vol. 105, no. 1, pp. 9–22, 2006.

[26] K. Suwanprasert, S. Seto, and S. Kaewrueng, "Intergrated drought risk indices from climate based and sattlelite based observation for agricultural drought monitoring in Thailand," *Journal of Japan Society of Civil Engineers, Ser. B1 (Hydraulic Engineering)*, vol. 69, no. 4, pp. 25–30, 2013.

[27] S. M. Quiring and S. Ganesh, "Evaluating the utility of the Vegetation Condition Index (VCI) for monitoring meteorological drought in Texas," *Agricultural and Forest Meteorology*, vol. 150, no. 3, pp. 330–339, 2010.

[28] K. Huang, C. Yi, D. Wu et al., "Tipping point of a conifer forest ecosystem under severe drought," *Environmental Research Letters*, vol. 10, no. 2, Article ID 024011, 2015.

[29] T. M. Scanlon, J. D. Albertson, K. K. Caylor, and C. A. Williams, "Determining land surface fractional cover from NDVI and rainfall time series for a savanna ecosystem," *Remote Sensing of Environment*, vol. 82, no. 2-3, pp. 376–388, 2002.

[30] S. M. Vicente-Serrano, C. Gouveia, J. J. Camarero et al., "Response of vegetation to drought time-scales across global land biomes," *Proceedings of the National Acadamy of Sciences of the United States of America*, vol. 110, no. 1, pp. 52–57, 2013.

[31] S. Beguería, S. M. Vicente-Serrano, and M. Angulo-Martínez, "A multiscalar global drought dataset: the SPEIbase: a new gridded product for the analysis of drought variability and impacts," *Bulletin of the American Meteorological Society*, vol. 91, no. 10, pp. 1351–1356, 2010.

[32] S. M. Vicente-Serrano, S. Beguería, and J. I. López-Moreno, "A multiscalar drought index sensitive to global warming: the standardized precipitation evapotranspiration index," *Journal of Climate*, vol. 23, no. 7, pp. 1696–1718, 2010.

[33] S. Beguería, S. M. Vicente-Serrano, F. Reig, and B. Latorre, "Standardized precipitation evapotranspiration index (SPEI) revisited: parameter fitting, evapotranspiration models, tools, datasets and drought monitoring," *International Journal of Climatology*, vol. 34, no. 10, pp. 3001–3023, 2014.

[34] Global SPEI database, 2016.

[35] F. Abramopoulos, C. Rosenzweig, and B. Choudhury, "Improved ground hydrology calculations for Global Climate Models (GCMs): soil water movement and evapotranspiration," *Journal of Climate*, vol. 1, no. 9, pp. 921–941, 1988.

[36] A. Grundstein, "Evaluation of climate change over the continental United States using a moisture index," *Climatic Change*, vol. 93, no. 1-2, pp. 103–115, 2009.

[37] C. D. Allen, D. D. Breshears, and N. G. McDowell, "On underestimation of global vulnerability to tree mortality and forest die-off from hotter drought in the Anthropocene," *Ecosphere*, vol. 6, no. 8, article 129, 2015.

[38] N. B. Guttman, "Accepting the standardized precipitation index: a calculation algorithm," *JAWRA Journal of the American Water Resources Association*, vol. 35, no. 2, pp. 311–322, 1999.

[39] M. Turco, A. Ceglar, C. Prodhomme, A. Soret, A. Toreti, and J. Doblas-Reyes Francisco, "Summer drought predictability over Europe: empirical versus dynamical forecasts," *Environmental Research Letters*, vol. 12, no. 8, p. 084006, 2017.

[40] C. F. Dewes, I. Rangwala, J. J. Barsugli, M. T. Hobbins, and S. Kumar, "Drought risk assessment under climate change is sensitive to methodological choices for the estimation of evaporative demand," *PLoS ONE*, vol. 12, no. 3, Article ID e0174045, 2017.

[41] NOAA, *Vegetation Health Product: Algorithm Description*, 41 NOAA. Vegetation health product, Algorithm description, 2016, http://www.ospo.noaa.gov/Products/land/vhp/algo.html.

[42] F. N. Kogan, "Application of vegetation index and brightness temperature for drought detection," *Advances in Space Research*, vol. 15, no. 11, pp. 91–100, 1995.

[43] I. Harris, P. D. Jones, T. J. Osborn, and D. H. Lister, "Updated high-resolution grids of monthly climatic observations—the CRU TS3.10 Dataset," *International Journal of Climatology*, vol. 34, no. 3, pp. 623–642, 2014.

[44] M. A. Friedl, D. K. McIver, J. C. F. Hodges et al., "Global land cover mapping from MODIS: algorithms and early results," *Remote Sensing of Environment*, vol. 83, no. 1-2, pp. 287–302, 2002.

[45] C. O. Justice, J. R. G. Townshend, E. F. Vermote et al., "An overview of MODIS Land data processing and product status," *Remote Sensing of Environment*, vol. 83, no. 1-2, pp. 3–15, 2002.

[46] D. C. Nepstad, C. R. De Carvalho, E. A. Davidson et al., "The role of deep roots in the hydrological and carbon cycles of Amazonian forests and pastures," *Nature*, vol. 372, no. 6507, pp. 666–669, 1994.

[47] I. T. Baker, L. Prihodko, A. S. Denning, M. Goulden, S. Miller, and H. R. Da Rocha, "Seasonal drought stress in the amazon: reconciling models and observations," *Journal of Geophysical Research: Biogeosciences*, vol. 113, no. 1, 2008.

[48] S. Abbas, J. E. Nichol, F. M. Qamer, and J. Xu, "Characterization of drought development through remote sensing: a case study in Central Yunnan, China," *Remote Sensing*, vol. 6, no. 6, pp. 4998–5018, 2014.

[49] J.-E. Lee, R. S. Oliveira, T. E. Dawson, and I. Fung, "Root functioning modifies seasonal climate," *Proceedings of the National Acadamy of Sciences of the United States of America*, vol. 102, no. 49, pp. 17576–17581, 2005.

[50] D. Markewitz, S. Devine, E. A. Davidson, P. Brando, and D. C. Nepstad, "Soil moisture depletion under simulated drought in the Amazon: impacts on deep root uptake," *New Phytologist*, vol. 187, no. 3, pp. 592–607, 2010.

[51] Y. Fan and G. Miguez-Macho, "Potential groundwater contribution to Amazon evapotranspiration," *Hydrology and Earth System Sciences*, vol. 14, no. 10, pp. 2039–2056, 2010.

[52] M. D. Vrettas and I. Y. Fung, "Sensitivity of transpiration to subsurface properties: exploration with a 1-D model," *Journal of Advances in Modeling Earth Systems*, vol. 9, no. 2, pp. 1030–1045, 2017.

[53] K. Ichii, H. Hashimoto, M. A. White et al., "Constraining rooting depths in tropical rainforests using satellite data and ecosystem modeling for accurate simulation of gross primary production seasonality," *GCB Bioenergy*, vol. 13, no. 1, pp. 67–77, 2007.

[54] K. Ichii, W. Wang, H. Hashimoto et al., "Refinement of rooting depths using satellite-based evapotranspiration seasonality for ecosystem modeling in California," *Agricultural and Forest Meteorology*, vol. 149, no. 11, pp. 1907–1918, 2009.

[55] R. R. Nemani, C. D. Keeling, H. Hashimoto et al., "Climate-driven increases in global terrestrial net primary production from 1982 to 1999," *Science*, vol. 300, no. 5625, pp. 1560–1563, 2003.

[56] N. Y. Krakauer and J. T. Randerson, "Do volcanic eruptions enhance or diminish net primary production? Evidence from tree rings," *Global Biogeochemical Cycles*, vol. 17, no. 4, pp. 29-1, 2003.

[57] A. R. Huete, K. Didan, Y. E. Shimabukuro et al., "Amazon rainforests green-up with sunlight in dry season," *Geophysical Research Letters*, vol. 33, no. 6, 2006.

[58] N. Y. Krakauer, B. I. Cook, and M. J. Puma, "Contribution of soil moisture feedback to hydroclimatic variability," *Hydrology and Earth System Sciences*, vol. 14, no. 3, pp. 505–520, 2010.

[59] B. I. Cook, M. J. Puma, and N. Y. Krakauer, "Irrigation induced surface cooling in the context of modern and increased greenhouse gas forcing," *Climate Dynamics*, vol. 37, no. 7-8, pp. 1587–1600, 2011.

[60] C. Yi, R. Li, J. Wolbeck et al., "Climate control of terrestrial carbon exchange across biomes and continents," *Environmental Research Letters*, vol. 5, no. 3, Article ID 034007, 2010.

[61] F. Kogan, W. Guo, and W. Yang, "SNPP/VIIRS vegetation health to assess 500 California drought," *Geomatics, Natural Hazards and Risk*, pp. 1–13, 2017.

[62] J. Rockström, "Resilience building and water demand management for drought mitigation," *Physics and Chemistry of the Earth, Parts A/B/C*, vol. 28, no. 20–27, pp. 869–877, 2003.

[63] M. van der Velde, G. Wriedt, and F. Bouraoui, "Estimating irrigation use and effects on maize yield during the 2003 heatwave in France," *Agriculture, Ecosystems & Environment*, vol. 135, no. 1-2, pp. 90–97, 2010.

[64] J. R. Kosgei, G. P. W. Jewitt, V. M. Kongo, and S. A. Lorentz, "The influence of tillage on field scale water fluxes and maize yields in semi-arid environments: a case study of Potshini catchment, South Africa," *Physics and Chemistry of the Earth*, vol. 32, no. 15-18, pp. 1117–1126, 2007.

[65] R. Lal, "Managing soil water to improve rainfed agriculture in India," *Journal of Sustainable Agriculture*, vol. 32, no. 1, pp. 51–75, 2008.

[66] J. I. L. Morison, N. R. Baker, P. M. Mullineaux, and W. J. Davies, "Improving water use in crop production," *Philosophical Transactions of the Royal Society B*, vol. 363, no. 1491, pp. 639–658, 2008.